

I. M. Ranieri and S. L. Baldochi

*Center for Lasers and Applications, Inst. Pesquisas Energeticas & Nucl.,
CP 11049, Butantã 05422-970, São Paulo, SP, Brazil*

D. Klimm*

Institute for Crystal Growth, Max-Born-Str. 2, 12489 Berlin, Germany

The Phase Diagram $\text{GdF}_3\text{--LuF}_3$

Abstract

The phase diagram gadolinium fluoride – lutetium fluoride was determined by differential scanning calorimetry (DSC) and X-ray powder diffraction analysis. Both pure components undergo a reversible first order transformation to a high temperature phase. The mutual solubility of both components is unlimited in the orthorhombic room temperature phase. The maximum solubility of Lu in the high temperature phase of GdF_3 (tysonite type) is about 20% and the maximum solubility of Gd in LuF_3 ($\alpha\text{-YF}_3$ type) is about 40%. Intermediate compositions of the low temperature phase decompose upon heating in a peritectoid reaction to a mixture of both high temperature phases.

Key words: phase diagram, solid solution, phase transformation

1. Introduction

Rare earth trifluorides (REF_3 , RE = La, Ce, ... Lu), including yttrium fluoride, were extensively studied in the past, instead of this many questions about the high-temperature polymorphic transformations and its structure so far remain. Oftedal [1,2] and Schlyter [3], determined the LaF_3 structure as hexagonal with the $P6_3/mcm$ space group and two formula units per elementary cell, using synthesized powder and the lanthanum mineral tysonite (= fluocerite). Mansmann [4,5] and at same time Zalkin et al. [6] established the current accepted structure of the LaF_3 . Using smaller X-ray wavelength (MoK_α) it was possible to observe weaker additional reflections on a single crystal,

and the structure of the LaF_3 tysonite structure was described as trigonal with space group $P\bar{3}c1$ and $Z = 6$. The light rare earths fluorides from La to Nd crystallize in this structure. All other rare earth fluorides crystallize at room temperature in the orthorhombic structure determined by Zalkin and Templeton [7] for YF_3 , also referred as $\beta\text{-YF}_3$, space group $Pnma$ and $Z = 4$.

Another characteristic pointed out by Mansmann for the change of the structure from trigonal to orthorhombic was due to a relation between the size of the metal and its coordination number. When the ionic radius of the rare earth r_{RE} decreases, the fluorine ions tend to touch each other, resulting in a repulsive energy. A critical ratio $r_{\text{RE}}/r_{\text{F}} = 0.94$ was proposed for the change from the LaF_3 to the $\alpha\text{-YF}_3$ structure, taking into account the ionic radius calculated by Ahrens [8]. Furthermore, the trigonal structure could be stabilized if the REF_3 -orthorhombic structure becomes deficient in fluorine ions or at high temperatures [5].

* Corresponding author: Tel.: +49 30 6392 3024; fax: +49 30 6392 3003.

Email addresses: iranieri@ipen.br (I. M. Ranieri), baldochi@ipen.br (S. L. Baldochi), klimm@ikz-berlin.de (D. Klimm).

Thoma et al. [9] studied the behavior of the REF_3 from SmF_3 to LuF_3 taking into account X-ray diffraction at high temperature and differential thermal analysis (DTA) experiments. It was observed that the REF_3 from Sm to Ho have the trigonal $P\bar{3}c1$ high- T structure of LaF_3 “tysonite” type mentioned above. For the small rare earths from Er to Lu upon heating, the $\beta\text{-YF}_3$ structure changes to a hexagonal not well identified $\alpha\text{-YF}_3$ structure. This structure was considered tentatively isostructural with the trigonal $\alpha\text{-UO}_3$ structure by Sobolev et al. [10,11], belonging to $P\bar{3}m1$ (D_{3d}^3) space group, $Z = 1$ [12]. Nevertheless, the $\alpha\text{-UO}_3$ structure is not yet well understood too. Either superstructures or a lower (e.g. orthorhombic) symmetry were discussed, as single crystal show a biaxial optical interference figure [13,14].

Jones and Shand [15] proved that it was possible to grow crystals of the four tysonites, LaF_3 , CeF_3 , PrF_3 and NdF_3 , but only the orthorhombic DyF_3 and HoF_3 using CdF_2 as scavenger. After Garton [16] and Pastor [17] it was established that GdF_3 , TbF_3 , DyF_3 and HoF_3 crystals can be grown from oxygen free compounds and in a reactive atmosphere, confirming the thermodynamic studies by Spedding et al [18].

For the intermediate SmF_3 , EuF_3 , and GdF_3 two subsequent transformations $Pnma \xrightarrow{(1)} P\bar{3}c1 \xrightarrow{(2)} P6_3/mmc$ were discussed by Greis [19] (the number in brackets indicates the order of the phase transformation [PT]). These PT were inferred from electron diffraction experiments with LaF_3 , where small synthesized crystals presented also sub-cells reflections as observed by Schlyter [3] and Maximov [20]. Stankus [21] claimed that at high T the $\beta\text{-YF}_3$ type ($Pnma$) and the LaF_3 type (tysonite, $P\bar{3}c1$) become practically identical. Sobolev et al. [22] constructed the phase diagrams of the systems $\text{GdF}_3\text{--LnF}_3$ ($\text{Ln} = \text{Tb, Ho, Er, Yb}$), solid solutions regions were proposed without phase transitions in all systems, when the cation mean ionic radius was between that of the Tb^{3+} and Er^{3+} .

Recently, the present authors have published a phase diagram study of the system $\text{GdF}_3\text{--YF}_3$ [23]. It was established that both components undergo a solid-state phase transformation of first order before melting. Additionally, a λ -shaped maximum of $c_p(T)$ being characteristic for a second order transformation was found for GdF_3 . Both low- T and high- T phases exhibit unlimited mutual solubility. This observation raises the question, whether the high-

T structures of YF_3 (reported as $P\bar{3}m1$) and GdF_3 (reported as $P6_3/mmc$) may really be different [10].

In the current paper, the phase diagram of the system $\text{GdF}_3\text{--LuF}_3$ is reported for the first time. The interest in this phase diagram derived from DTA studies regarding the phase diagram of the system $\text{LiF--Gd}_{1-x}\text{Lu}_x\text{F}_3$, which is interesting to develop new solid-solution crystals of the type $\text{LiGd}_{1-x}\text{Lu}_x\text{F}_4$ to be used as laser host.

2. Experimental

Mixtures of $\text{Gd}_{1-x}\text{Lu}_x\text{F}_3$ with $x = 0.2, 0.4, 0.6$ and 0.8 , respectively, were prepared using commercial LuF_3 (AC Materials, 6N purity) and GdF_3 synthesized from commercial Gd_2O_3 powder (Alfa, 5N purity) by hydrofluorination. The oxide was placed in a platinum boat inside a platinum tube, and slowly heated in a stream of argon gas (White Martins, purity 99.995%) and HF gas (Matheson Products, purity 99.99%) up to 850°C . This process is described in detail elsewhere [24,25]. Conversion rates $> 99.9\%$ of the theoretical value calculated for the reaction $\text{Gd}_2\text{O}_3 + 6\text{HF} \rightarrow 2\text{GdF}_3 + 3\text{H}_2\text{O}$ were measured by comparing the masses prior to and after the hydrofluorination process. These samples were used to the DSC measurements.

Thermoanalytic measurements were performed with a NETZSCH STA 409CD with DSC/TG sample carrier (thermocouples type S). The sample carrier was calibrated for T and sensitivity at the phase transformation points of BaCO_3 and at the melting points of Zn and Au. Sample powders (50 – 70 mg) were placed in graphite DSC crucibles with lid. As graphite is not wetted by the molten fluorides, the melt forms one single almost spherical drop (diameter $d \approx 3$ mm) that could be used for the subsequent X-ray phase analysis.

The vapor pressures of both fluorides at their melting points are high. Fortunately, the evaporation rate for pure GdF_3 or LuF_3 , respectively, was found to be almost identical. Thus it can be assumed that the partial evaporation does not lead to a considerable concentration shift. The inhomogeneous powder samples were homogenized in a first heating/cooling cycle with ± 40 K/min. Here the heating was performed to that T_{max} where the DSC melting peak was just finished and the molten sample could homogenize. Depending on x , this was the case for $1145^\circ\text{C} \leq T_{\text{max}} \leq 1280^\circ\text{C}$ and due to the large heating rate the mass loss did never exceed

4% in these preliminary mixing cycles. Without intermediate opening of the apparatus, the mixing cycle was followed by a measuring run with a heating rate of 10 K/min. Although the crucibles were covered by lids, the evaporation of $\approx 10 - 15\%$ sample mass during this DSC/TG run cannot be avoided. Cooling curves showed often supercooling and were not used for the construction of the phase diagram. In total, 14 different compositions ranging from pure GdF_3 ($x = 0$) to pure LuF_3 ($x = 1$) were measured.

Other samples were melted under a flux of hydrogen fluoride gas, then pulverized to be analyzed by powder X-ray diffraction, using a Bruker AXS diffractometer, model D8 Advance, operated at 40 kV and 30 mA, in the 2θ range of $22.5 - 68.5^\circ$. The diffraction patterns were treated with the Rietveld Method [26] using the GSAS program to calculate the lattice parameters [27].

3. Results and Discussion

It turned out that GdF_3 as well as LuF_3 showed similar DSC heating curves: A first endothermal peak due to the first order PT ($T_{\text{PT}}^{\text{GdF}_3} = 902^\circ\text{C}$ or $T_{\text{PT}}^{\text{LuF}_3} = 946^\circ\text{C}$, respectively) is followed by a second endothermal peak due to melting ($T_{\text{f}}^{\text{GdF}_3} = 1252^\circ\text{C}$ or $T_{\text{f}}^{\text{LuF}_3} = 1182^\circ\text{C}$, respectively). The values for GdF_3 were measured and compared with literature data recently [23], and for lutetium fluoride one finds values $943 \leq T_{\text{PT}}^{\text{LuF}_3} \leq 963$ and $1180 \leq T_{\text{f}}^{\text{LuF}_3} \leq 1188$ (T in $^\circ\text{C}$) in the literature [9,19,21]. Only Jones & Sand [15] reported the very low value $T_{\text{PT}}^{\text{LuF}_3} \approx 874^\circ\text{C}$. Like in the recent study [23] weak λ shaped bends were found in the DSC curves of GdF_3 rich mixtures with $x < 0.2$. This could be an indication for a second order transformation between T_{PT} and T_{f} but will not be discussed here.

Fig. 1 shows DSC heating curves for five compositions starting from pure LuF_3 ($x = 1.0$) to $\text{Gd}_{0.6}\text{Lu}_{0.4}\text{F}_3$. The PT peak for $x = 1.0$ is disturbed by a shoulder on the low T side that is assumed to result from some contamination of the sample, as no additional peak that could be related to the presence of oxyfluorides was detected on cooling. With increasing GdF_3 content the melting peak shifts to lower T until it reaches for $x \approx 0.6$ the constant value $T_{\text{eut}} = 1092^\circ\text{C}$. On the contrary, the PT peak shifts with increasing GdF_3 content to higher T and reaches for $x \approx 0.5$ the constant value $T_{\text{PT}} = 1051^\circ\text{C}$. The same T_{PT} and T_{eut} are reached

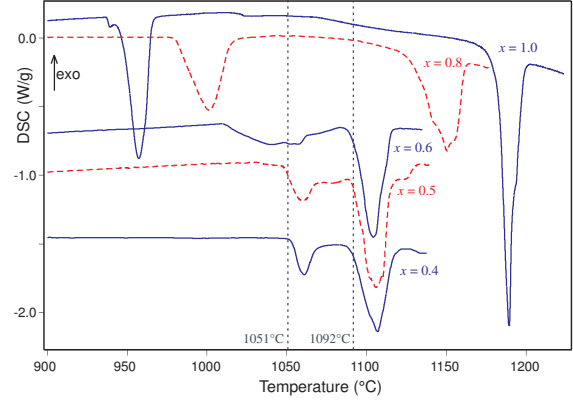


Fig. 1. DSC curves (2nd heating with 10 K/min) of LuF_3 ($x = 1.0$) and of four mixtures $\text{Gd}_{1-x}\text{Lu}_x\text{F}_3$ with $0.4 \leq x \leq 0.8$. $T_{\text{PT}} = 1051^\circ\text{C}$ and $T_{\text{eut}} = 1092^\circ\text{C}$ are the two isothermal phase boundaries in Fig. 4.

if one starts with pure GdF_3 and adds LuF_3 .

The lattice constants of nine samples with initial LuF_3 concentrations $0 \leq x_0 \leq 1$ were measured by X-ray diffraction. All diffraction patterns were fitted considering the orthorhombic structure with the $Pnma$ space group, no parasitic peaks that would indicate the presence of other phases were observed at room temperature (Fig. 2). The experimental errors $\{\Delta a_0, \Delta b_0, \Delta c_0\}$ were always $\leq 5 \times 10^{-4} \text{ \AA}$ but were found to be maximum in the region $0.2 \leq x_0 \leq 0.4$. Fig. 3 shows the total error $\sigma = \Delta a_0 + \Delta b_0 + \Delta c_0$ versus the LuF_3 concentration x_0 of the sample, together with a_0, b_0, c_0 .

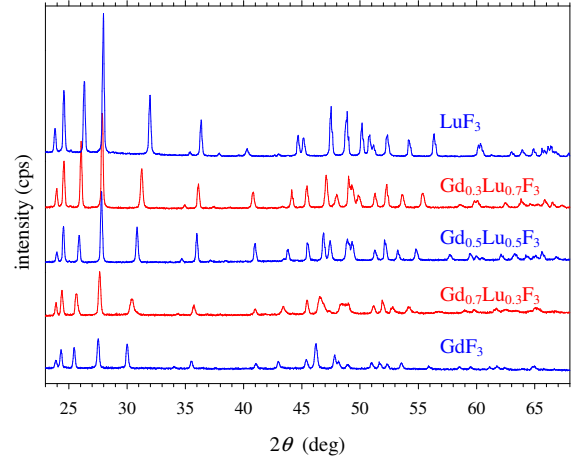


Fig. 2. Diffractions patterns of some $\text{Gd}_{1-x}\text{Lu}_x\text{F}_3$ samples utilized to determine the lattice parameters at room temperature.

Table 1 reports the results for calculated values of a_0, b_0 and c_0 , the volume of the unit cell V , the mass density ρ and the mean rare-earth ionic radius in

the solid solution $\bar{r} = (1 - x_0)r_{\text{Gd}}^{[8]} + x_0 r_{\text{Lu}}^{[8]}$ and $r_{\text{Lu}}^{[8]}$ are the ionic radii of Gd^{3+} and Lu^{3+} , respectively, with coordination number 8 as determined by Shannon et al. [28].

Table 1

Lattice parameters for the $Pnma$ phase of $\text{Gd}_{1-x}\text{Lu}_x\text{F}_3$ ($0 \leq x \leq 1$)

Lu content \bar{r} (x , molar)	a_0 (Å)	b_0 (Å)	c_0 (Å)	V (Å ³)	ρ (g/cm ³)	
0.00	6.571 ^a	6.984 ^a	4.390 ^a	201.47 ^a	7.063 ^a	
0.00	1.053	6.5758(2)	6.9898(2)	4.3947(2)	201.999(11)	7.045
0.20	1.038	6.5143(6)	6.9517(5)	4.3907(3)	198.833(31)	7.157
0.25	1.034	6.4908(4)	6.9429(3)	4.3964(2)	198.125(18)	7.331
0.30	1.030	6.4671(5)	6.9209(4)	4.3918(2)	196.569(28)	7.359
0.40	1.023	6.4102(3)	6.8867(2)	4.3885(1)	193.733(13)	7.588
0.50	1.015	6.3838(2)	6.8770(2)	4.4025(1)	193.275(8)	7.667
0.60	1.007	6.3421(2)	6.8615(2)	4.4154(2)	192.143(11)	7.773
0.70	1.000	6.2855(2)	6.8222(1)	4.4140(1)	189.282(10)	7.967
1.00	0.977	6.1481(2)	6.7640(2)	4.4732(1)	186.021(11)	8.283
1.00	6.150 ^b	6.760 ^b	4.468 ^b	185.83 ^b	8.291 ^b	

^a PDF 49-1804; ^b PDF 32-0612

The lattice parameters a_0 and b_0 drop linearly with x_0 and c_0 is almost constant for $x_0 \leq 0.4$ and starts then to rise slightly up to the value of pure LuF_3 (Fig. 3). The smooth variation of a_0 , b_0 and c_0 over the whole concentration range is obviously the result of unlimited mutual solubility of GdF_3 and LuF_3 in their low- T phases. The variation of c_0 in this system is very similar to the c axis variation of the pure rare earth fluorides. In the orthorhombic rare-earth fluorides due to the lanthanides contraction, there is a linear decreasing in the c_0 parameter value from 4.40 Å (SmF_3) down to 4.376 Å (DyF_3) and then a nearly exponential increase up to 4.467 Å (LuF_3) [7]. Taking into account the ionic radius of Ho^{3+} , namely 1.015 Å (with a coordination number of 8) [28], and the mean ionic radius of the composition $\text{Gd}_{0.5}\text{Lu}_{0.5}\text{F}_3$, one has the same value.

The DSC and XRD results are summarized in Fig. 4 where full circles represent experimental DSC points that could be well determined by extrapolated onsets of sharp peaks. Such points represent the lower boundary of PT regions or, in the case of melting, the solidus line. The higher boundary of PT regions or the liquidus line, respectively, are less remarkable as here the PT process or melting just finishes and the DSC curve returns to the basis line.

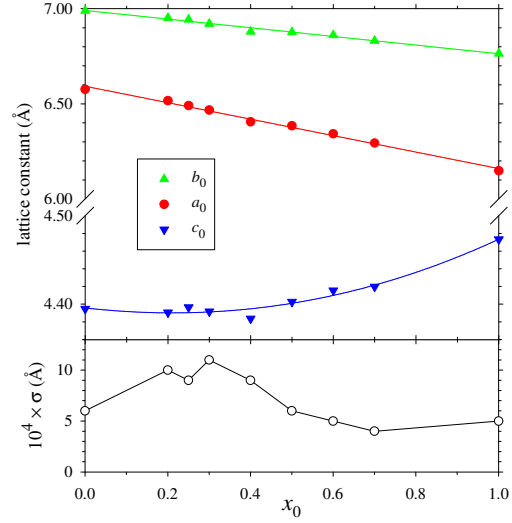


Fig. 3. Top: lattice constants for the $Pnma$ phase (β - YF_3 type) of $\text{Gd}_{1-x}\text{Lu}_x\text{F}_3$ solid solutions at room temperature. Bottom: experimental error $\sigma = \Delta a_0 + \Delta b_0 + \Delta c_0$.

Such more vague determined events are marked by hollow circles in Fig. 4.

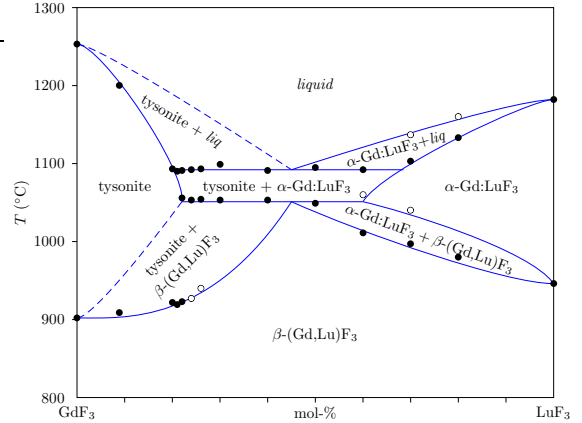
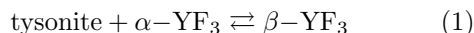


Fig. 4. Phase diagram GdF_3 - LuF_3 . ● – sharp peaks. ○ – small peaks or from offsets. α , β mean high- T phase or low- T phase, respectively.

Two horizontal lines at $1051 \pm 2^\circ\text{C}$ and $1092 \pm 2^\circ\text{C}$ are the most prominent feature of the experimental phase diagram Fig. 4. Obviously, two different processes with strong thermal effects start independent on composition x for a broad range $0.2 \lesssim x \lesssim 0.5 \dots 0.6$ always at the same $T_{\text{PT}} = 1051^\circ\text{C}$ or $T_{\text{eut}} = 1092^\circ\text{C}$, respectively. The components GdF_3 and LuF_3 show complete miscibility in the liquid phase. If the melt is cooled, either Gd-saturated LuF_3 (α - YF_3 type, $P\bar{3}m1$) or Lu-saturated GdF_3 (tysonite type, $P6_3/mmc$ or $P\bar{3}c1$) crystallize from the melt. Both high- T phases belong to different

space groups and unlimited miscibility is therefore prohibited — instead a eutectic is formed below 1092 °C. In the eutectic mixture between T_{eut} and T_{PT} both constituents are mutually saturated. In the β -phase both components exhibit unlimited mutual solubility. The phase transformation occurring at T_{PT} for medium concentrations x



is a peritectoid reaction.

Near the left or right rims of the phase diagram, single phase Lu-doped GdF_3 (tysonite structure) as well as single phase Gd-doped LuF_3 ($= \alpha\text{-Gd:LuF}_3$) transform upon cooling to $\beta\text{-(Gd,Lu)F}_3$, crossing a 2-phase field where α - and β -phase are mixed and the upper and lower limit of this 2-phase field depend on x . Both 2-phase fields “tysonite + liq.” and “tysonite + $\beta\text{-(Gd,Lu)F}_3$ ” are broader than the corresponding fields on the LuF_3 rich side where tysonite is replaced by $\alpha\text{-Gd:LuF}_3$. The larger widths of the 2-phase fields on the GdF_3 rich side may result in stronger phase segregation of such compositions, resulting after cooling to room temperature in microscopic grains with a wider variation of compositions. As different compositions of the $\text{Gd}_{1-x}\text{Lu}_x\text{F}_3$ grains result in different lattice constants, the larger experimental error σ that is observed for Gd-rich mixtures (but not for pure GdF_3) can be explained by variations of x resulting from segregation.

4. Conclusion

Solid solutions $\text{Gd}_{1-x}\text{Lu}_x\text{F}_3$ are formed over the whole concentration range $0 \leq x \leq 1$ and crystallize in the same $\beta\text{-YF}_3$ type structure with space group $Pnma$ like the pure components GdF_3 and LuF_3 . Upon heating GdF_3 undergoes a first order phase transformation to a tysonite type structure whereas LuF_3 undergoes a first order transformation to a $\alpha\text{-YF}_3$ type structure that is not isomorphous to tysonite. As a result, a miscibility gap separates the high- T phases of GdF_3 and LuF_3 . For intermediate compositions $0.2 \lesssim x \lesssim 0.6$ the phase transformation from single phase $\text{Gd}_{1-x}\text{Lu}_x\text{F}_3$ to a mixture of the high- T phases of GdF_3 (saturated with Lu) and LuF_3 (saturated with Gd) is a peritectoid decomposition.

The behavior of the system $\text{GdF}_3\text{--LuF}_3$ is somewhat uncommon: Usually the mutual solubility of components rises with T , but in the present case both components show unlimited miscibility in the

low- T phase only. It should be noted that Nafziger et al. [29] obtained similar results (constant eutectic and phase transformation temperatures $T_{\text{eut}} = 1073$ °C and $T_{\text{PT}} = 1045$ °C, respectively, over an extended composition range $\gtrsim 50\%$) with DTA measurements in the $\text{LaF}_3\text{--YF}_3$ system. Nafziger et al. speculated that this is an indication for a low- T intermediate phase, but the present authors think that a peritectoid decomposition (1) as shown in Fig. 4 of this work would be a more simple explanation and that the postulation of an (otherwise not proven) intermediate phase is not necessary.

Acknowledgements

The authors acknowledge financial support from CAPES (grant number 246/06) and DAAD (grant number D/05/30364) in the framework of the PROBRAL program.

References

- [1] I. Oftedal, Z. Physik. Chem. B 5 (1929) 272–291.
- [2] I. Oftedal, Z. Physik. Chem. 13 (1931) 190–200.
- [3] K. Schlyter, Arkiv för kemi 5 (1953) 73–82.
- [4] M. Mansmann, Z. anorg. allg. Chem. 331 (1964) 98–101, doi:10.1002/zaac.19643310115.
- [5] M. Mansmann, Z. Kristallogr. 122 (1965) 375–398.
- [6] A. Zalkin, D. H. Templeton, T. E. Hopkins, Inorg. Chem. 5 (1966) 1466–1468, doi:10.1021/ic50042a047.
- [7] A. Zalkin, D. H. Templeton, J. Amer. Chem. Soc. 75 (1953) 2453–2458, doi:10.1021/ja01106a052.
- [8] L. H. Ahrens, Geochim. Cosmochim. Acta 2 (1952) 155–169, doi:10.1016/0016-7037(52)90004-5.
- [9] R. E. Thoma, G. D. Brunton, Inorg. Chem. 5 (1966) 1937–1939, doi:10.1021/ic50045a022.
- [10] B. P. Sobolev, P. P. Fedorov, Sov. Phys. Crystallogr. 18 (1973) 392.
- [11] B. P. Sobolev, P. P. Fedorov, D. B. Shteynberg, B. V. Sinitsyn, G. S. Shakhkalamian, J. Solid State Chem. 17 (1976) 191–199, doi:10.1016/0022-4596(76)90220-6.
- [12] W. H. Zachariasen, Acta Cryst. 1 (1948) 256–268, doi:10.1107/S0365110X48000703.
- [13] C. Greaves, B. E. F. Fender, Acta Cryst. B 28 (1972) 3609–3614, doi:10.1107/S056774087200843X.
- [14] S. Siegel, H. R. Hoekstra, Inorg. Nucl. Chem. Lett. 7 (1971) 497–504, doi:10.1016/0020-1650(71)80238-6.
- [15] D. A. Jones, W. A. Shand, J. Crystal Growth 2 (1968) 361–368, doi:10.1016/0022-0248(68)90029-8.
- [16] G. Garton, P. J. Walker, Mat. Res. Bull. 13 (1978) 129–133, doi:10.1016/0025-5408(78)90077-6.
- [17] R. C. Pastor, M. Robinson, Mat. Res. Bull. 9 (1974) 569–578, doi:10.1016/0025-5408(74)90126-3.

- [18] F. H. Spedding, B. J. Beaudry, D. C. Henderson, J. Moorman, J. Chem. Phys. 60 (1974) 1578–1588, doi:10.1063/1.1681233.
- [19] O. Greis, M. S. R. Cader, *thermochimica acta* 87 (1985) 145–150, doi:10.1016/0040-6031(85)85329-6.
- [20] B. Maximov, H. Schulz, *Acta Cryst. B* 41 (1985) 88–91, doi:10.1107/S0108768185001677.
- [21] S. V. Stankus, R. A. Khairulin, K. M. Lyapunov, *High Temperatures – High Pressures* 32 (2000) 467–472, doi:10.1068/htwu216.
- [22] D. F. Sobolev, V. S. Sidorov, P. P. Fedorov, D. D. Ikrami, *Sov. Phys. Crystallogr.* 22 (1977) 574–577.
- [23] D. Klimm, I. M. Ranieri, R. Bertram, S. L. Baldochi, *Mat. Res. Bull.* 42, doi:10.1016/j.materresbull.2007.04.004.
- [24] H. Guggenheim, *J. Appl. Phys.* 34 (1963) 2482–2485, doi:10.1063/1.1702768, see also: R. Bougon, J. Ehretsmann, J. Portier, A. Tressaud, in P. Hagenmuller (Ed.): *Preparative Methods in Solid State Chemistry*, Academic Press, New York, 1972, p. 401.
- [25] I. M. Ranieri, Growth of $\text{LiY}_{1-x}\text{TR}_x\text{F}_4\text{:Nd}$ (TR = Lu or Gd) crystals for optical applications, Ph.D. thesis, IPEN/University of São Paulo (2001).
- [26] H. M. Rietveld, *J. Appl. Cryst.* 2 (1969) 65–71, doi:10.1107/S0021889869006558.
- [27] A. C. Larson, R. B. V. Dreele, General structure analysis system (GSAS), Tech. Rep. LAUR 86-748, Los Alamos National Laboratory (2007).
- [28] R. D. Shannon, *Acta Cryst. A* 32 (1976) 751–767, doi:10.1107/S0567739476001551.
- [29] R. H. Nafziger, R. L. Lincoln, N. Riazance, *J. inorg. nucl. Chem.* 35 (1973) 421–426, doi:10.1016/0022-1902(73)80553-6.